Geoscience Letters

RESEARCH LETTER

Open Access

Origin of the 30–60-day intraseasonal oscillation of streamflow in source region of Yellow River in China: a perspective of the atmospheric signals from mid-high latitude

Lun Li[1,2], Congwen Zhu[1*], Xiangde Xu[1], Ziyan Zheng[3], Shuangmei Ma[1] and Wanyi Sun[1]

Abstract

Streamflow in source region of Yellow River (SRYR) matters with regard to the adjacent and downstream water resources. Intraseasonal oscillation (ISO) in the streamflow in SRYR is of great significance to the sub-seasonal prediction of streamflow in SRYR, but is unknown. Here, we first report a 30–60-day ISO in the streamflow in SRYR, which is regulated by the atmospheric 30–60-day ISO at mid-high latitude over North Eurasia. The 30–60-day ISO in atmosphere is featured by a Rossby wavetrain, and the wave energy propagates southward onto the TP, which causes anomalous wind response over TP. The leading anomalous high (low) with anti-cyclonic (cyclonic) wind anomalies over the TP favors dry (wet) air in lower troposphere in SRYR, via enhancing the water vapor divergence (convergence). Dry (wet) air always results in strong (weak) evaporation from the Yellow River, which causes the later streamflow valley (peak) and thereby the 30–60-day ISO in the streamflow in SRYR.

Keywords Tibetan Plateau, Streamflow, Source region of Yellow River, 30–60-day intraseasonal oscillation

Introduction

Yellow River is the second greatest river in China, it originates from the Tibetan Plateau (TP) and serves as the most important water source in North China. The source region of Yellow River (SRYR) is located in the northeastern TP, where the streamflow accounts for nearly 40% of the total annual amount in the Yellow River, and plays a very important role in water resource supply along the Yellow River basin (Hu et al. 2011; Wu et al. 2018; Jin et al. 2022; Lan et al. 2004). Multi-timescale variability of streamflow in SRYR greatly matters to the downstream industries, domestic households and agriculture. Therefore, fully understanding the streamflow variability in SRYR will benefit the social-economic development, water management, as well as its multi-timescale climate forecast.

The source of streamflow in SRYR mainly comes from the surrounding precipitation, melting ice, snow and permafrost, as well as the subsurface water (Jia et al. 2008; Lan et al. 2010a; 2010b). The climate change, and human activities including land use, vegetation destruction, water resource facilities, are important factors affecting the variability of streamflow in SRYR (Liang et al. 2015; Piao et al. 2010; Wang et al. 2009). Of which, the

*Correspondence:
Congwen Zhu
zhucw@cma.gov.cn
[1] State Key Laboratory of Severe Weather, Chinese Academy of Meteorological Sciences, Beijing, China
[2] Collaborative Innovation Center on Forecast and Evaluation of Meteorological Disasters (CIC-FEMD), Nanjing University of Information Science and Technology, Nanjing, China
[3] Institute of Atmospheric Physics, Chinese Academy Science, Beijing, China

local precipitation, air temperature and evaporation is regarded as the three dominant meteorological variables influencing the streamflow in SRYR (Shi et al. 2007; Wang et al. 2012; Lv et al. 2015). However, responses of the streamflow to the precipitation and temperature are diverse at different timescales in distinct reaches of Yellow River (Labat 2010; Su et al. 2017; Lan et al. 2010a, b; Jiang and Li 2011; Chiew et al. 1995; Kamga 2001; Zhang et al. 2007).

The streamflow in SRYR shows a robust seasonal cycle, with the largest amount in summer and the smallest in winter (Bai et al. 2016; Jiang and Li 2011). There is a decreasing trend in the streamflow in SRYR since 1960s (Li et al. 2012; Lan et al. 2010a; Zhang et al. 2017; Chu et al. 2018; Hu et al. 2021; Shi et al. 2017; Yang et al. 2021, 2023), and the streamflow exhibits an increasing trend since 2000 (Shi et al. 2007; Bao et al. 2021; Zhang et al. 2020; Jiang and Li 2011). In addition, the streamflow in SRYR shows an irregular interannual and decadal oscillation, with the periods of 3–4, 5–8, 15–18, 22–25, and 42 years, depending on the study periods and methods used to detect the periods (Ma 1995; Hou et al. 2020; Jiang and Li 2011; Li et al. 2012; Chu et al. 2018).

As stated above, the linear trend, decadal, interannual, and seasonal variations in streamflow in SRYR have been widely discussed (see the preceding paragraph). But, few attentions have been paid to the variability of streamflow in SRYR at intraseasonal (or sub-seasonal) timescale. The intraseasonal oscillation (ISO) is referred to as the 10–90-day variability in surface air temperature, rainfall, and atmospheric variables. This timescale bridges the synoptic and seasonal climate variability, and is regarded as the important target of sub-seasonal prediction (Vitart et al. 2015). However, in contrast to the ISO in surface air temperature and rainfall, the ISO in streamflow in SRYR is less known. Accordingly, in the present work, we intend to explore the ISO in the streamflow. Here we find a 30–60-day ISO in streamflow in SRYR that cannot be explained by surrounding precipitation. Therefore, we will focus on the 30–60-day ISO in streamflow in SRYR and try to reveal the underlying mechanism.

Data and method

TangNaiHai hydrological station (TNH) is located in the upstream of Yellow River (Fig. 1a), the streamflow at which is rarely affected by human activities and mainly determined by meteorological factors (Bai et al. 2016; Zhang et al. 2017). It has been suggested that the variation in streamflow at TNH performs well in representing the change in streamflow in SRYR (Hu et al. 2011; Wu et al. 2018; Jin et al. 2022; Lan et al. 2004). Here we use the daily observed streamflow at TNH to reveal the intraseasonal variability of the streamflow in SRYR. The daily observed streamflow covering May–August of 1997–2018 is provided by the Yellow River Conservancy Commission of the Ministry of Water Resources. The daily atmospheric components are calculated from the hourly ERA5 reanalysis of the European Centre for Medium-Range Weather Forecasts (ECMWF), with a resolution of $0.25°\times0.25°$ (Hersbach et al. 2020). The daily rain gauge observed precipitation at 13 stations along the Yellow River in SRYR is provided by the information center of China Meteorological Administration (CMA), and the total rainfall amount at the 13 stations is considered as the income of streamflow in SRYR.

We calculate the power spectrums of the streamflow at TNH and the rainfall amount in SRYR to detect the dominant ISO signals. In addition, we apply a band-pass filter method of Lanczos (Duchon 1979) to extract the ISO components. The mean square deviation (MSD) of the band-pass filtered variable is used to measure the ISO intensity. Furthermore, we calculate the wave activity flux (WAF) (Takaya and Nakamura 2001; Tam and Li 2006) to explore the wave activity at intraseasonal timescales. The WAF equation given in Takaya and Nakamura (2001) is shown as follows:

$$\mathbf{W}=\frac{p\cos\phi}{2|\mathbf{U}|}\begin{pmatrix}\frac{U}{a^2\cos^2\phi}\left[\left(\frac{\partial\psi'}{\partial\lambda}\right)^2-\psi'\frac{\partial^2\psi'}{\partial\lambda^2}\right]+\frac{V}{a^2\cos\phi}\left[\frac{\partial\psi'}{\partial\lambda}\frac{\partial\psi'}{\partial\phi}-\psi'\frac{\partial^2\psi'}{\partial\lambda\partial\phi}\right]\\ \frac{U}{a^2\cos\phi}\left[\frac{\partial\psi'}{\partial\lambda}\frac{\partial\psi'}{\partial\phi}-\psi'\frac{\partial^2\psi'}{\partial\lambda\partial\phi}\right]+\frac{V}{a^2}\left[\left(\frac{\partial\psi'}{\partial\phi}\right)^2-\psi'\frac{\partial^2\psi'}{\partial\phi^2}\right]\\ \frac{f_0^2}{N^2}\left\{\frac{U}{a\cos\phi}\left[\frac{\partial\psi'}{\partial\lambda}\frac{\partial\psi'}{\partial z}-\psi'\frac{\partial^2\psi'}{\partial\lambda\partial z}\right]+\frac{V}{a}\left[\frac{\partial\psi'}{\partial\phi}\frac{\partial\psi'}{\partial z}-\psi'\frac{\partial^2\psi'}{\partial\phi\partial z}\right]\right\}\end{pmatrix}+C_UM.$$

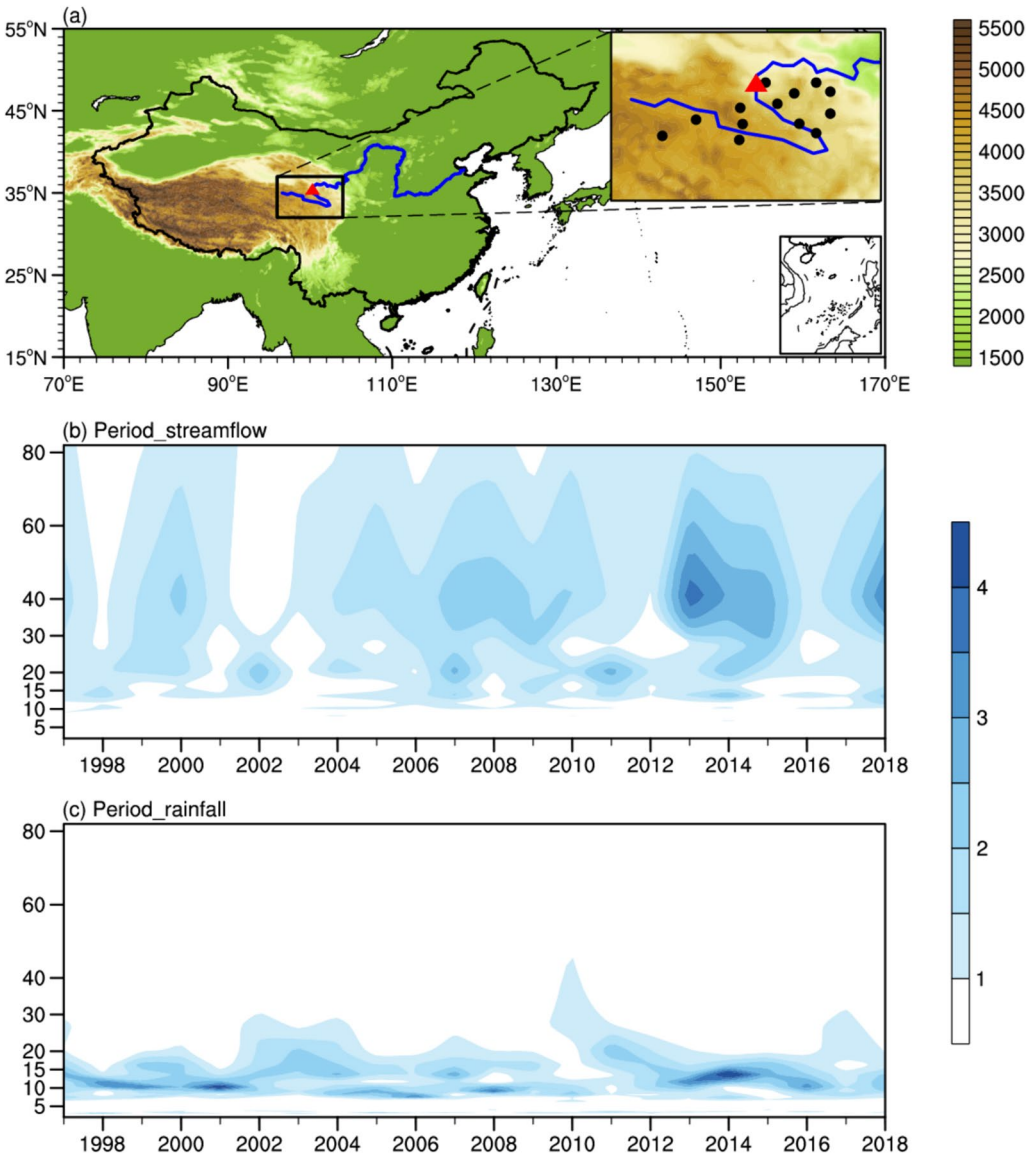

Fig. 1 **a** Locations of the Yellow River (blue line) and TNH (red triangle). The shadings represent the elevation, and TP is the area with elevation higher than 3000 m. **b** Ratios of the power spectrum of the streamflow at TNH to the red noise spectrum at α = 0.05 significance level. **c** Ratios of the power spectrum of the precipitation in SRYR to the red noise spectrum at α = 0.05 significance level. In **b** and **c**, values greater than 1 indicate the periods passing 95% confidence level. Y-axis and x-axis denote the period (unit: day) and time (unit: year), respectively

W is the phase-independent wave-activity flux, p = (pressure/1000 hPa), ψ' is perturbation stream function. a is the earth's radius, ϕ and λ are latitude and longitude, respectively. U and V are zonal and meridional basic flow, respectively. **U** indicates the vector of a steady zonally inhomogeneous basic flow. N^2 is the buoyancy frequency squared. C_U is the vector that represents the phase propagation in the direction of **U**, and the calculation formula of quantity M can be found in Eqs. 26 and 27 in Takaya and Nakamura (2001). The other symbols are of conventional use in meteorology. The detailed introduction for the WAF equation can be found in Takaya and Nakamura (2001).

Eight phases of the 30–60-day ISO in streamflow in SRYR are identified by conducting the following steps. First, 30–60-day ISO component of the streamflow in SRYR is extracted by using the 30–60-day band-pass filter, and then the filtered series is standardized. Second, peaks and valleys of the filtered streamflow are identified, and the peak phases are recorded as phase 1 and valley phases as phase 5. Third, times between the peak and valley phases, at which the filtered streamflow equals zero (simply as "zero times"), are detected,

and the zero times following the peak (valley) times are recorded as phase 3 (phase 7). Fourth, times in the middle between phases 1 and 3 are defined as phase 2, and those between phases 5 and 7 are defined as phase 6.

In order to reveal the causation of the ISO in streamflow in SRYR, the environmental conditions before the valley and peak phases of the filtered streamflow in SRYR are analyzed.

Original signal of 30–60-day ISO in streamflow in SRYR

Figure 1b and c shows the ratios of the power spectrum of streamflow at TNH and precipitation in SRYR to the red noise spectrum at $\alpha = 0.05$ significance level. The values in Fig. 1b and c greater than 1.0 imply the periods exceeding 95% significance level. Significant 10–20-day and 30–60-day ISO are detected in streamflow at TNH (Fig. 1b). The 10–20-day ISO in streamflow can be explained by the counterpart of precipitation, however, the 30–60-day ISO in streamflow cannot be resembled by the counterpart of precipitation (Fig. 1c). We speculate this 30–60-day ISO in streamflow is mainly originated from the local land–atmospheric interaction.

To explore the origination of atmospheric 30–60-day ISO, we calculate the atmospheric ISO intensity and WAF. The average MSDs of the 30–60-day filtered geopotential height at the near surface level over the TP (550 hPa) during May–August of 1997–2018 is shown in Fig. 2a. Stronger 30–60-day ISO in geopotential height appears at mid-high latitude with the largest MSDs being over northwest of the TP. Relatively weak 30–60-day ISO is observed over the northern TP. Actually, atmospheric 30–60-day ISO at mid-high latitudes was

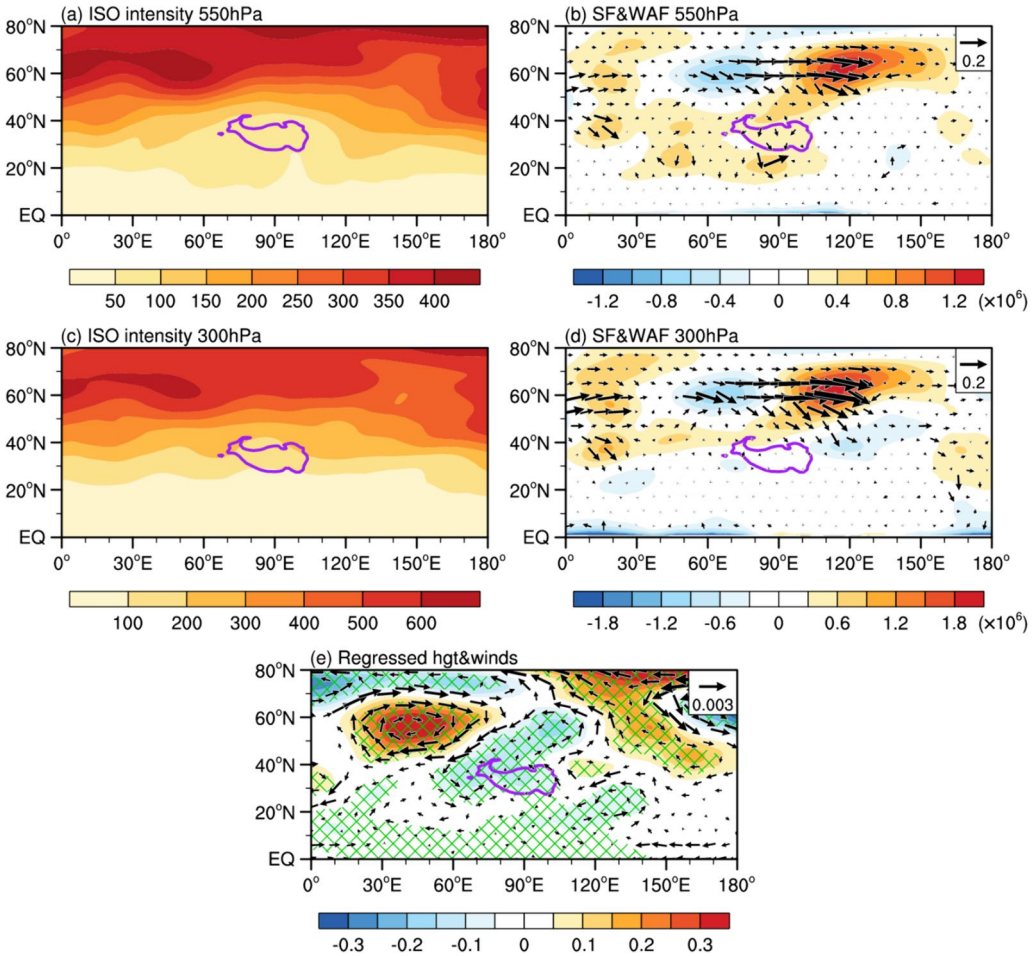

Fig. 2 Average MSDs of the 30–60-day filtered geopotential height during May–August of 1997–2018 at **a** 550 hPa and **c** 300 hPa. WAF (vectors; unit: $m^2\ s^{-2}$) and stream function (shadings; unit: $m^2\ s^{-1}$) in phases 2–4 of the 30–60-day ISO in streamflow at TNH at **b** 550 hPa and **d** 300 hPa. **e** Regressions of the 550-hPa geopotential height (shadings) and wind (vectors) against the annually averaged streamflow at TNH during May to August. In **e**, the regressed geopotential height with the statistical significance exceeding 95% confidence level is marked by green lattices, and only the regressed wind passing 95% confidence level is shown. In **a**–**e**, the thick purple lines represent the topographic contours of 3000 m

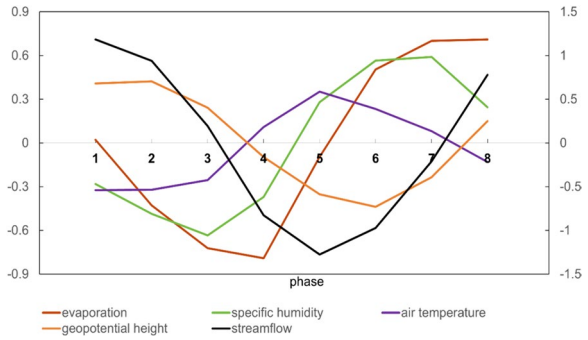

Fig. 3 Eight phases of the 30–60-day ISO in streamflow at TNH (x-axis) based on the standardized 30–60-day filtered streamflow at TNH (black; y-axis on the right), and the standardized 30–60-day filtered geopotential height (orange; y-axis on the left), mean evaporation rate (brown; y-axis on the left), specific humidity (green; y-axis on the left), and air temperature (purple; y-axis on the left) averaged in SRYR (96–103°E, 33–35°N) at each phase of the streamflow

firstly discovered in 1980s (Anderson and Rosen 1983; Krishnamurti and Gadgil 1985; Zhang 1987), and two primary circulation patterns were reported in Li (1990), i.e., Eurasian-Pacific teleconnection pattern and Pacific-North America pattern. The WAF indicates the propagation of the wave energy at 550 hPa (Fig. 2b). Because WAF is independent on ISO phases (Takaya and Nakamura 2001), the distributions of WAF are similar in each phase of the 30–60-day ISO in streamflow in SRYR. Thus, WAF in phases 2–4 (the 8 phases of ISO in streamflow are shown in Fig. 3) are illustrated in Fig. 2b for example. Wave energy of the strongest 30–60-day ISO at mid-high latitude northwest of the TP generally propagates eastward north of the TP, with a branch propagating southward onto the TP, implying that the 30–60-day ISO over the northern TP is attributed to the wave energy propagating from the mid-high latitude. Similar distribution of the ISO intensity and propagation of the wave energy are also observed in upper troposphere (Fig. 2c and d). Regressions of the 550-hPa geopotential height and wind against the annual streamflow at TNH averaged during May to August are provided in Fig. 2e. An anomalous high with anti-cyclonic wind is observed northwest of the TP at mid-high latitude, and anomalously low appears over the TP, accompanied by cyclonic wind. Therefore, large (small) streamflow in SRYR corresponds to anomalous high (low) northwest of the TP at mid-high latitude and anomalous low (high) over the TP, and the anomalous high (low) northwest of the TP fall in the area with the strongest 30–60-day ISO (Fig. 2a).

Eight phases are defined based on the standardized 30–60-day filtered streamflow at TNH (black line in Fig. 3), among which phase 1 corresponds to the peak of 30–60-day ISO in streamflow at TNH and phase 5 the valley. Accordingly, regional averaged circulation regime in 96–103°E, 33–35°N, covering the SRYR, at each phase of 30–60-day ISO in streamflow at TNH is shown in Fig. 3. Note that negative value of the mean evaporation rate in ERA5 data represents evaporation and positive value represents condensation. It is observed that the strongest (weakest) of evaporation appears at phase 4 (phase 8), which leads the valley (peak) of the streamflow for 1 phase, implying that the 30–60-day ISO in the streamflow is possible a response to the variation in evaporation. Air temperature and humidity are two primary factors affecting the evaporation. The air temperature varies synchronously with the streamflow, but the specific humidity reaches the valley (peak) at phase 3 (phase 7), which leads the strongest (weakest) evaporation for 1 phase. This demonstrates that the leading variation in specific humidity is responsible for the late response in evaporation. Furthermore, the valley (peak) of specific humidity follows the peak (valley) of the geopotential height at phase 2 (phase 6), which implies the important role of atmospheric circulation in modulating the specific humidity. The above sequence implies a possible chain effect producing the 30–60-day ISO in streamflow at TNH, which initiates from the atmospheric circulation anomalies.

Mechanism of 30–60-day ISO in streamflow in SRYR

Here we select valley and peak phases of the 30–60-day filtered streamflow at TNH, which are simply referred as valley and peak phases of the streamflow, respectively, hereafter. In order to explore the alternation between the valleys and peaks of the streamflow, we analyzed the leading environmental conditions of the valley (peak) phase of the streamflow (Fig. 4). Accordingly, composites of variables in phases 2–4 and phases 6–8 are provided in Fig. 4 for investigating the causations of the valleys and peaks of the streamflow, respectively.

Figure 4a and b shows the composites of 30–60-day filtered geopotential height and wind at 550 hPa. Ahead of the valley phase of the streamflow (Fig. 4a), there is an anomalous low located northwest of the TP and an anomalous high northeast of the TP, corresponding to the two wave activity centers at mid-high latitude (Fig. 2b). In addition, an anomalous high appears over the TP, which enhances the northerly wind anomalies over the TP and the anti-cyclonic wind divergence in northeastern TP. Similarly, ahead of the peak phase of the streamflow (Fig. 4b), the changes in geopotential height and wind anomalies lead to cyclonic wind convergence in northeastern TP. The composites of 30–60-day filtered vertically integrated water vapor flux and water vapor flux divergence are provided in Fig. 4c and d. Ahead of

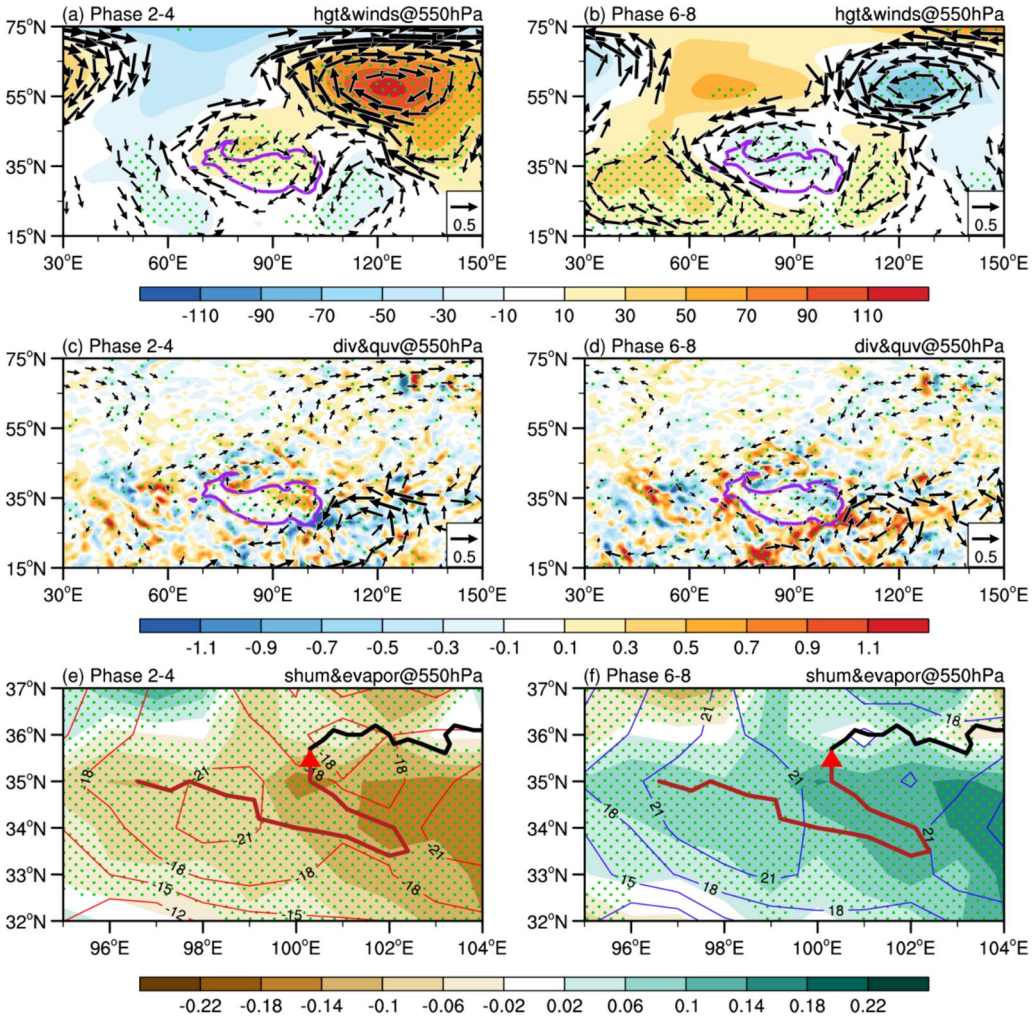

Fig. 4 Composites of 30–60-day filtered environmental conditions in **a**, **c**, **e** phases 2–4 (i.e., 1–3 phases ahead of the valley phase) and **b**, **d**, **f** phases 6–8 (i.e., 1–3 phases ahead of the peak phase) of the 30–60-day ISO in streamflow at TNH. **a** and **b** Geopotential height (shadings; unit: gpm) and wind (vectors; unit: m s^{-1}) at 550 hPa; the areas with the geopotential height passing the 95% confidence level are dotted, and only the wind vectors passing the 95% confidence level are plotted. **c** and **d** Vertically integrated water vapor flux (vectors; unit: kg m^{-1} s^{-1}) and water vapor flux divergence (shadings; unit: 10^{-5} kg m^{-2} s^{-1}); only the water vapor flux exceeding 95% confidence level are shown, and the areas with water vapor flux divergence exceeding 95% confidence level are marked by green dots. **e** and **f** Specific humidity (contours; unit: 10^{-5} kg kg^{-1}) at 550 hPa and the mean evaporation rate (shadings; unit: kg m^{-2} s^{-1}); the areas with evaporation rate exceeding 95% confidence level are marked by green dots; the red triangles represent the location of TNH; the thick red and black lines represent the Yellow River, in which the red lines indicate the section upstream TNH and the black lines represent the section downstream TNH. The thick purple lines in **a**–**d** represent the topographic contours of 3000 m

the valley phase of the streamflow (Fig. 4c), the water vapor is transported southward over the TP, and diverges in northeastern TP, especially in SRYR. In contrast, ahead of the peak phase of the streamflow (Fig. 4d), the water vapor is transported northward over the TP and converges in SRYR. Distribution of the water vapor flux over and around the TP coincides well with that of the wind fields at 550 hPa (Fig. 4a and b), implying that the water vapor conditions in SRYR mainly determined by the lower-level wind over the TP.

Because anomalous water vapor conditions can greatly affect the atmospheric humidity, and the latter is a crucial factor modulating the evaporation, the specific humidity and evaporation in SRYR are subsequently investigated. Composites of 30–60-day filtered specific humidity at 550 hPa and the surface mean evaporation rate are shown in Fig. 4e and f. Ahead of the valley phase of the streamflow (Fig. 4e), anomalously dry air in lower troposphere is observed in SRYR, which is favorable for the evaporation from the Yellow River. Correspondingly, evaporation

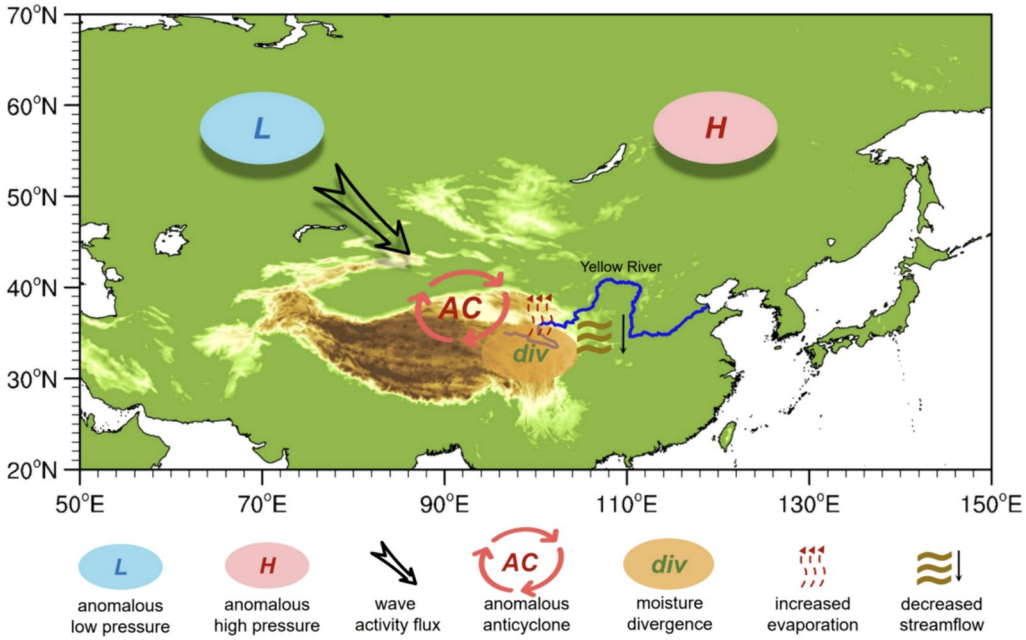

Fig. 5 Schematic diagram of the physical mechanism for the valley of the streamflow at TNH, and that for the peak is just the opposite

anomalies (negative values) appear along the Yellow River upstream TNH, resulting in more water loss in this section of the Yellow River and thereby the later valley of the streamflow. The specific humidity and the evaporation ahead of the peak phase of the streamflow are the opposite of those ahead of the valley phase (Fig. 4f). That is, anomalously wet air and condensation (positive values) are found in SRYR ahead of the peak phase, reducing the water loss in upstream Yellow River and thereby contributing to the later peak of the streamflow. Eventually, the alternation between the valleys and peaks of the streamflow at intraseasonal timescale is produced.

The underlying mechanism of the ISO in streamflow in SRYR is summarized in the schematic diagram (Fig. 5). In Fig. 5, only the physical mechanism for the valley of the streamflow is illustrated, and that for the peak is just the opposite but not displayed. The atmospheric 30–60-day ISO at mid-high latitude propagates southward onto the TP, leading to distinct wind fields over the TP ahead of the valley (peak) phase of the streamflow. The anomalous high (low) over the TP favor the dry (wet) air in lower troposphere via enhancing the water vapor divergence (convergence) in SRYR. The dry (wet) air induces local strong (weak) evaporation, which results in the later valley (peak) of the streamflow at TNH, and thereby the 30–60-day ISO in the streamflow in SRYR.

Conclusions and discussion

Conclusion

ISO is the important basis of sub-seasonal prediction, but the ISO in streamflow in SRYR is unknown. Here we find a 30–60-day ISO in streamflow in SRYR, which is not regulated by the contribution of precipitation. Our results show that the 30–60-day ISO signal of streamflow is originated from the atmospheric 30–60-day ISO at mid-high latitude over North Eurasia.

The energy of atmospheric 30–60-day ISO at mid-high latitude propagates southward onto the TP, leading to weak atmospheric 30–60-day ISO over the northern TP. The maximum (minimum) of the geopotential height, minimum (maximum) of the specific humidity, and the strongest (weakest) evaporation appear 3, 2, and 1 phase ahead of the valley (peak) phase of the streamflow at TNH, respectively. This kind of chronological sequence implies the causal relationships between the elements above, i.e., the changes in atmospheric circulation are responsible for the variations in atmospheric humidity, then the latter affects the evaporation from the Yellow River, and finally the streamflow is modulated. Furthermore, the specific underlying mechanism of the alternation between the valleys and peaks of the streamflow is investigated, by analyzing the leading environmental conditions of the valley and peak phases of the streamflow.

Anomalous high appears over the TP in lower troposphere over the TP, accompanied by anti-cyclonic wind divergence. The wind divergence leads to anomalous water vapor divergence in SRYR, which induces local anomalously dry air. Dry air enhances the evaporation from the river, and thereby results in more water loss of the river. The physical process above consequently contributes to the subsequent valley of the streamflow at TNH. The mechanism for the peak of the streamflow at TNH is just the opposite. In this fashion, the 30–60-day ISO in the streamflow at TNH is produced.

It has been shown the atmospheric nonlinear interaction (Li 1990; Yang and Cao 1995) and topographic forcing (Luo and Li 2000; Yan 1998) are thought greatly contributing the atmospheric 30–60-day ISO at mid-high latitude.

Discussion

Given the streamflow is a temporal accumulation and spatial integral of runoff over the river source region, the 30–60-day ISO in streamflow is possibly coming from the accumulated effect of 10–20-day and seasonal variation in precipitation. On 10–20-day time scale, the lag-lead correlation analyses indicates that the streamflow in SRYR is closely related to the precipitation 5–10 days earlier. Actually, the peak of precipitation leads the peak of streamflow for about 3 phases on 10–20-day time scale; the interannual variance of 10–20-day precipitation during May–August is significantly correlated with that in streamflow. These imply the dominant contribution of accumulated effect of precipitation to the streamflow on 10–20-day time scale. However, the correlation coefficient of 10–20-day precipitation with 30–60-day streamflow in SRYR is merely 0.13, implying the weak contribution of 10–20-day precipitation to 30–60-day streamflow. Furthermore, we examined the 10–20-day filtered precipitation at 8 phases of the 30–60-day ISO in streamflow. Our results show there is no robust lag/lead relationship between the 10–20-day ISO in precipitation and the 30–60-day ISO in streamflow (figures are not shown).

The 30–60-day ISO in streamflow mainly occurs in rainy season, and its peak phase lags the maximum precipitation in climatology. On interannual variability, the peak phase of the 30–60-day streamflow is significantly correlated with that of the maximum precipitation. This implies that the peak of the 30–60-day streamflow comes late (early) when the precipitation peak happens late (early). However, no significant correlation is observed between the amplitude of maximum precipitation and that of the maximum 30–60-day filtered streamflow, implying that the seasonal precipitation has little contribution to the amplitude of the 30–60-day ISO in streamflow.

Abbreviations

SRYR	Streamflow in source region of Yellow River
TP	Tibetan Plateau
ISO	Intraseasonal oscillation
TNH	TangNaiHai hydrological station
MSD	Mean square deviation
WAF	Wave activity flux
ECMWF	European Centre for Medium-Range Weather Forecasts
CMA	China Meteorological Administration

Acknowledgements

Not applicable.

Author contributions

Lun Li and Congwen Zhu designed the work and wrote the draft. Lun Li interpreted the data and analyzed. Xiangde Xu revised the draft. Ziyan Zheng and Shuangmei Ma processed the data. Wanyi Sun processed the figures.

Funding

This work is supported by the Second Tibetan Plateau Scientific Expedition and Research (STEP) program (Grant No. 2019QZKK0105), National Key Research and Development Program (Grant No. 2023YFC3007502), Heavy Rain and Drought-Flood Disasters in Plateau and Basin Key Laboratory of Sichuan Province (Grant No. SZKT202202), International Partnership Program of the Chinese Academy of Sciences (Grant No. 060GJHZ2022057MI), Basic Scientific Research and Operation Foundation of CAMS (Grants No. 2023Z024 & 2023Z003), Science and Technology Development Fund of CAMS (Grant No. 2023KJ009), and Special project for innovation and development of CMA (Grant No. CXFZ2023J050).

Availability of data and materials

ERA5 reanalysis provided by ECMWF can be accessed on Copernicus Climate Data Store (Copernicus Climate Change Service. (2019). ERA5 hourly data on pressure levels from 1959 to present. [Data set]. ECMWF. https://doi.org/https://doi.org/10.24381/cds.bd0915c6). The observed daily streamflow data at TNH are provided by the Yellow River Conservancy Commission of the Ministry of Water Resources (http://61.163.88.227:8006/hwsq.aspx?sr=0nkRxv6s9CTRMlwRgmfFF6jTpJPtAv87), which can be downloaded after application. Observational precipitation data from CMA can be obtained by applying to China National Meteorological Information Center, CMA (contact information is available at http://data.cma.cn/article/getLeft/id/251/keyIndex/6.html), with reasonable request.

Declarations

Competing interests

The authors declare that they have no competing interests.

Received: 2 April 2024 Accepted: 22 July 2024
Published online: 05 August 2024

References

Anderson JR, Rosen RD (1983) The latitude-height structure of 40–50 day variation in atmospheric angular momentum. J Atmos Sci 40:1584–1591

Bai X, Wang YM, Qi XM, Chai J, Yang L (2016) Analysis of statistical characteristics and evolution law of runoff in the upper Yellow River. Yellow River 9:1–7

Bao GY, Nie H, Dai S, Yan ZN, Yang CH, Dai QC (2021) Research on effects of different precipitation magnitudes on runoff changes in the headwater region of the upper Yellow River. Arid Zone Res 38:704–713

Chiew FH, Whetton PH, McMahon TA, Pittock AB (1995) Simulation of the impacts of climate change on runoff and soil moisture in Australian catchment. J Hydrol 167:121–147

Chu HB, Wei JH, Li JY, Li TJ (2018) Investigation of the relationship between runoff and atmospheric oscillations, sea surface temperature, and local-scale climate variables in the Yellow River headwaters region. Hydrol Process 32:1434–1448
Duchon CE (1979) Lanczos filtering in one and two dimensions. J Appl Meteorol 18:1016–1022
Hersbach H, Coauthors (2020) The ERA5 global reanalysis. Q J R Meteorol Soc 146:1999–2049
Hou BF, Jiang C, Sun OJX (2020) Differential changes in precipitation and runoff discharge during 1958–2017 in the headwater region of Yellow River of China. J Geogr Sci 30:1401–1418
Hu Y, Maskey S, Uhlenbrook S, Zhao H (2011) Streamflow trends and climate linkages in the source region of the Yellow River. China Hydrol Processes 25:3399–3411
Hu YM, Liang ZM, Solomatine DP, Wang HM, Liu T (2021) Assessing the impact of precipitation change on design annual runoff in the headwater region of Yellow River, China. J Environ Inf 37:122–129
Jia YW, Gao H, Niu CW, Qu YQ (2008) Impact of climate change on runoff process in headwater area of the Yellow River. J Hydraul Eng 39:52–58
Jiang YC, Li DL (2011) Variations of Tangnaihai runoff and precipitation and temperature in the upper reach of the yellow river. Meteorol Disaster Reduct Res 34:51–57
Jin XY, Jin HJ, Luo DL, Sheng Y, Wu QB, Wu JC, Wang WH, Huang S, Li XY, Liang SH, Wang QF, He RX, Serban DR, Ma Q, Gao SH, Li Y (2022) Impacts of permafrost degradation on hydrology and vegetation in the source area of the Yellow River on northeastern Qinghai-Tibet Plateau, southwest China. Front Earth Sci 10:845824
Kamga FM (2001) Impact of greenhouse gas induced climate change on the runoff of the Upper Banue River (Cameroon). J Hydrol 252:145–156
Krishnamurti TN, Gadgil S (1985) On the structure of the 30 to 50 day mode over the global during FGGE. Tellus 37A:336–360
Labat D (2010) Cross wavelet analyses of annual continental freshwater discharge and selected climate indices. J Hydrol 385:269–278
Lan YC, Ding YJ, Zhu YT, Ma JH, Wei Z (2004) Possible change on the runoff in the upper Yellow River Basin under global warming scenarios. J Glaciol Geocryol 26:668–673
Lan YC, Wen J, Zhao GH, Shen YP, Hu XL, Chang JJ, Ma JH (2010a) Sensibility analysis of the runoff in the headwater regions of the Yellow River to climate change. J Glaciol Geocryol 32:175–182
Lan YC, Zhao GH, Zhang YN, Wen J, Hu XL, Liu JQ, Gu ML, Chang JJ, Ma JH (2010b) Response of runoff in the headwater region of the Yellow River to climate change and its sensitivity analysis. J Geogr Sci 20:848–860
Li CY (1990) Intraseasonal oscillation in the atmosphere. Chin J Atmos Sci 1990(14):32–45
Li L, Shen HY, Dai S, Xiao JS, Shi XH (2012) Response of runoff to climate change and its future tendency in the source region of Yellow River. J Geogr Sci 22:431–440
Liang W, Bai D, Wang F, Fu B, Yan J, Wang S, Yang Y, Long DI, Feng M (2015) Quantifying the impacts of climate change and ecological restoration on streamflow changes based on a Budyko hydrological model in China's Loess Plateau. Water Resour Res 51:6500–6519
Luo DH, Li CY (2000) Near-resonant interactions between slowly moving Rossby waves and large-scale topography. Chin J Atmos Sci 24:271–283
Lv JQ, Shen B, Li HE, Jiang Y (2015) Study on the runoff response to climate change-a case study of source region of the Yellow River. J Hydroelectr Eng 34:191–198
Ma ZG (1995) The characteristics of the temporal variation of flow-off at Tang Naihai and Ge Zhouba. Plateau Meteorol 14:19–27
Piao SL, Ciais P, Huang Y, Shen ZH, Peng SS, Li JS, Zhou LP, Liu HY, Ma YM, Ding YH, Friedlingstein P, Liu CZ, Tan K, Yu YQ, Zhang TY, Fang JY (2010) The impacts of climate change on water resources and agriculture in China. Nature 467:43–51
Shi XH, Qin NS, Wang QC, Qian YH, Feng SQ, Yang GL, Liu QC (2007) Analysis on runoff variation characteristics and influencing factors in the upper Yellow River. J Desert Res 27:690–697
Shi HL, Hu CH, Wang YG, Liu C, Li HM (2017) Analyses of trends and causes for variations in runoff and sediment load of the Yellow River. Int J Sedim Res 32:171–179
Su L, Miao CY, Borthwick AG, Duan Q (2017) Wavelet-based variability of Yellow River discharge at 500-, 100-, and 50-year timescales. Gondwana Res 49:94–105
Takaya K, Nakamura H (2001) A formation of a phase-independent wave-activity flux for stationary and migratory quasigeostrophic eddies on a zonally varying basic flow. J Atmos Sci 58:608–627
Tam CY, Li T (2006) The origin and dispersion characteristics of the observed tropical summertime synoptic-scale waves over the western Pacific. Mon Weather Rev 134:1630–1646
Vitart F, Robertson AW, S2S Steering Group (2015) Sub-seasonal to seasonal prediction: Linking weather and climate. In: Brunet G, Jones S, Ruti PM (eds) Seamless Prediction of the Earth System: From Minutes to Months, WMO-1156. World Meteorological Organization, Geneva, pp 385–401
Wang GS, Xia J, Chen J (2009) Quantification of effects of climate variations and human activities on runoff by a monthly water balance model: a case study of the Chaobai River basin in northern China. Water Resour Res 45(W00A11):1–12
Wang SJ, Yan M, Yan YX, Shi CX, He L (2012) Contributions of climate change and human activities to the changes in runoff increment in different sections of the Yellow River. Quatern Int 282:66–77
Wu X, Zhang X, Xiang X, Zhang K, Hua W (2018) Changing runoff generation in the source area of the Yellow River: Mechanisms, seasonal patterns and trends. Cold Reg Sci Technol 155:58–68
Yan BL (1998) Topographic forcing role in the 30–60 day oscillation in the high latitudes. Chin J Atmos Sci 22:169–177
Yang DS, Cao WZ (1995) A possible dynamic mechanism of the atmospheric 30–60 day period oscillation in the extratropical latitude. Chin J Atmos Sci 19:209–218
Yang MD, Liu H, Han YP, Zeng QH, Wang JH, Hu P (2021) Temporal and spatial changes of runoff regime in the Yellow River basin from 1956 to 2017. Water 13:3298
Yang JJ, Wang TH, Yang DW, Yang YT (2023) Insights into runoff changes in the source region of Yellow River under frozen ground degradation. J Hydrol 617:128892
Zhang KS (1987) The 40–50 day low-frequency oscillation of the zonal mean flow and its destabilizing effect. Chin J Atmos Sci 1987(11):227–236
Zhang GH, Fu SH, Fang WH, Imura H, Zhang XC (2007) Potential effects of climate change on runoff in the Yellow River basin of China. Trans ASABE 50:911–918
Zhang YY, Hu YP, Zhang FP (2017) The Characteristics of natural streamflow in the upstream of the Yellow River. J Arid Land Resour Environ 31:104–109
Zhang JP, Li HB, Sun B, Fang HY (2020) Annual runoff prediction in the source area of the Yellow River based on structure change co-integration theory. Water Supply 20:1664–1677

Publisher's Note